Dyes and Pigments 189 (2021) 109238

Contents lists available at ScienceDirect

Dyes and Pigments

journal homepage: http://www.elsevier.com/locate/dyepig

FRET processes of bi-fluorophoric sensor material containing tetraphenylethylene donor and optical-switchable merocyanine acceptor for lead ion (Pb^{2+}) detection in semi-aqueous media

Feng-Cheng Ho [a,b], Kuan-Hsiang Huang [a,b], Hung-Wei Cheng [a,b], Yi-Jing Huang [a,b], Pham Quoc Nhien [a,b,c], Chia-Hua Wu [a,b], Judy I. Wu [d], San-Yuan Chen [a,b], Hong-Cheu Lin [a,b,e,*]

[a] Department of Materials Science and Engineering, National Chiao Tung University, Hsinchu, 300, Taiwan
[b] Department of Materials Science and Engineering, National Yang Ming Chiao Tung University, Hsinchu, 300, Taiwan
[c] Department of Chemistry, College of Natural Sciences, Can Tho University, Can Tho City, 94000, Viet Nam
[d] Department of Chemistry, University of Houston, Houston, TX, 77204, United States
[e] Center for Emergent Functional Matter Science, National Yang Ming Chiao Tung University, Hsinchu 300, Taiwan

ARTICLE INFO

Keywords:
Aggregation-induced emission (AIE)
Bi-fluorophoric sensor
Förster resonance energy transfer (FRET)
Optical-switchable

ABSTRACT

A novel aggregation-induced emission (AIE) structure containing a tetraphenylethene (TPE) unit covalently linked with a spiropyran (SP) unit was synthesized and investigated in semi-aqueous solutions with 90% water fraction. The open-form structure of red-emissive merocyanine (MC) unit combined with TPE unit was utilized as a bi-fluorophoric sensor to detect lead(II) ion, which could be transformed from the close-form structure of non-emissive SP unit upon UV exposure. Moreover, the TPE unit as an energy donor with the blue-green photoluminescence (PL) emission at 480 nm was combined with the MC unit as an energy acceptor with the red PL emission at 635 nm. Due to the Förster resonance energy transfer (FRET) processes, the bi-fluorophoric sensor produced more efficient ratiometric PL behavior to induce a stronger red PL emission than that of the mono-fluorophoric MC unit. Hence, the PL sensor responses of the AIE bi-fluorophoric structure toward lead(II) ion could be further amplified via the FRET-OFF processes to turn off red PL emission of the coordinated MC acceptor and to recover blue-green PL emission of the TPE donor. Accordingly, the best LOD value for the AIE sensor detection toward Pb^{2+} was 0.27 μM. The highest red MC emission with the optimum FRET process of AIE sensor could be utilized in cell viability tests to prove the non-toxic and remarkable bio-marker of AIE sensor to detect lead(II) ion in live cells. The developed FRET-OFF processes with ratiometric PL behavior of the bi-fluorophoric AIE sensor can be utilized for future chemo- and bio-sensor applications.

1. Introduction

Heavy metals, for example nickel (Ni), chromium (Cr), cadmium (Cd), lead (Pb), copper (Cu) and zinc (Zn), in industrial wastewater have been a major source of contamination to our environment [1,2]. Among them, lead (Pb) is the most commonly-found pollutant in soil [3], water and air due to its usage in many commercial processes, such as construction, piping systems, lead-acid batteries, solder and radiation shielding. Upon consuming, lead poisoning can cause irreversible damages in human body, including brain and kidney anemia, severe stomach pain, muscle weakness and other related genetic diseases. The maximum allowable concentration of lead ions in drinking water is 4.8 μM according to World Health Organization (WHO)'s guideline [4]. Although many instruments for Pb^{2+} detection have been developed for practical applications, there are few reports on highly-selective, rapid and low-cost lead ion detection methods. Since fluorescent sensors have played one of the important roles in detecting metal ions in recent years [5–7], the interests of developing novel fluorescent sensor probes toward lead ion detection have grown significantly. So far, the recognition of Pb^{2+} via the electrostatic interaction and chelation are normally utilized for fluorescent lead ion sensors [8]. For instance, some electrostatic interaction [9] and chelation examples [10] can be used as turn-on and turn-off fluorescent Pb^{2+} sensor probes. Due to the negative charge on the open merocyanine (MC) form by UV exposure [11–13], it

* Corresponding author. Department of Materials Science and Engineering, National Yang Ming Chiao Tung University, Hsinchu 300, Taiwan.
E-mail address: linhc@mail.nctu.edu.tw (H.-C. Lin).

https://doi.org/10.1016/j.dyepig.2021.109238
Received 30 December 2020; Received in revised form 9 February 2021; Accepted 9 February 2021
Available online 21 February 2021

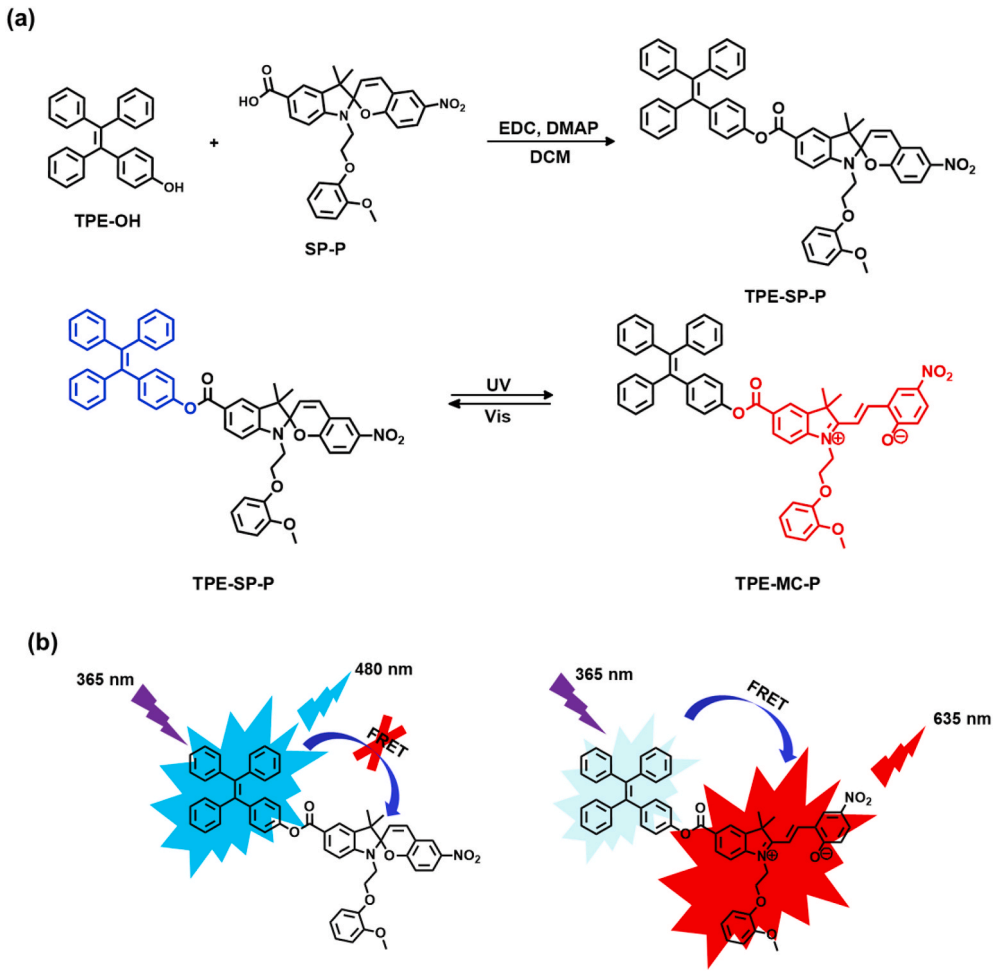

Scheme 1. (a) Synthetic routes of **(TPE-SP-P)** and **(TPE-MC-P)** (b) cartoon illustration of FRET effect upon UV/Vis exposure.

can induce the properties of aggregation induced emission (AIE) easily along with the enhanced water solubility, which lead to efficient detection of lead ions in aqueous media [14].

Nowadays, smart materials have received many attentions, owing to their numerous physical properties (light, pH, temperature and pressure) sensitive to external stimuli [15–18]. With distinctive photochromic properties in smart materials, molecules can exhibit different absorptions, structures and other characteristics upon UV–Vis irradiation [19,20]. The molecular designs in various applications, such as mechanical arms [21–23], textile, sensors [24] and safe labels [25,26], have explored the possibilities of incorporating the photochromic properties, including optical switchable fluorescent structures containing diarylethene [27], spiropyran [28] (SP), azobenzene [29], overcrowded ethene. Among them, spiropyran-based materials have been widely studied because of their rapid response, high sensitivity and modifiability. Upon UV and visible light exposures, the close SP unit can undergo reversible isomerization processes and transfer to the open MC unit. The SP to MC isomerization can also be triggered by different external stimuli, in particular, solvent [30], acid/base [31], temperature [32], metal ion, and mechanical force.

Fluorescence switches have attracted many interests in sensor developments recently, due to their advantages of fast response time, high sensitivity and good selectivity [33]. However, for traditional fluorescent dyes, PL emissions can only be observed in specific organic solvents or dilute solutions. In the conditions of high concentrations or solid states, most planar fluorescent molecules prefer strong π-π stacking interactions, resulting in aggregation caused quench (ACQ) phenomena [34–36]. Another type of fluorescence switching, developed by Tang and coworker in 2001, takes advantages of AIE phenomena [37–39], which show strong PL emissions in their aggregation states due to the restriction of their rotational degrees of freedom upon the self-assembly of TPE units.

Among many AIE systems, including distyreneanthracene (DSA) [40], hexaphenylsilole (HPS) [41], tetraphenylethylene (TPE) unit shows promising potentials. A variety of TPE derivatives with AIE properties have been synthesized and show excellent efficiency and sensitivity. These derivatives can be incorporated in chemical sensors [42], biological probes [43–45], drug deliveries [46] and hydrogels as well as many practical applications in different fields. In addition, the combination of TPE and other ACQ fluorophores will facilitate various AIE effects which are able to achieve high emission efficiencies easily [47]. Förster resonance energy transfer (FRET) is recognized a radiative energy transfer process, and it is widely applied in fluorescent sensing and energy harvesting [48,49]. Upon photoexcitation, the excited state donor can transfer the energy to ground state acceptor chromophore through dipole-dipole coupling. As a highly distance-dependent process, FRET requires a suitable donor-acceptor distance to be smaller than 10 nm, which requires the significant overlap of the donor emission to the acceptor absorption spectrum [50]. In fluorescent sensing, PL emission sensitivities are essential to be detected by subtle changes of analyte concentrations [51,52]. The contrast of ratiometric emissions in a bi-fluorophoric system can be magnified via triggering the FRET process between two fluorophores [53]. Therefore, the FRET ON/OFF mechanism is extensively used in sensor applications, including medical diagnosis [54], biological analysis [55], and optical imaging [56].

As shown in Scheme 1, we have designed and synthesized a mono-

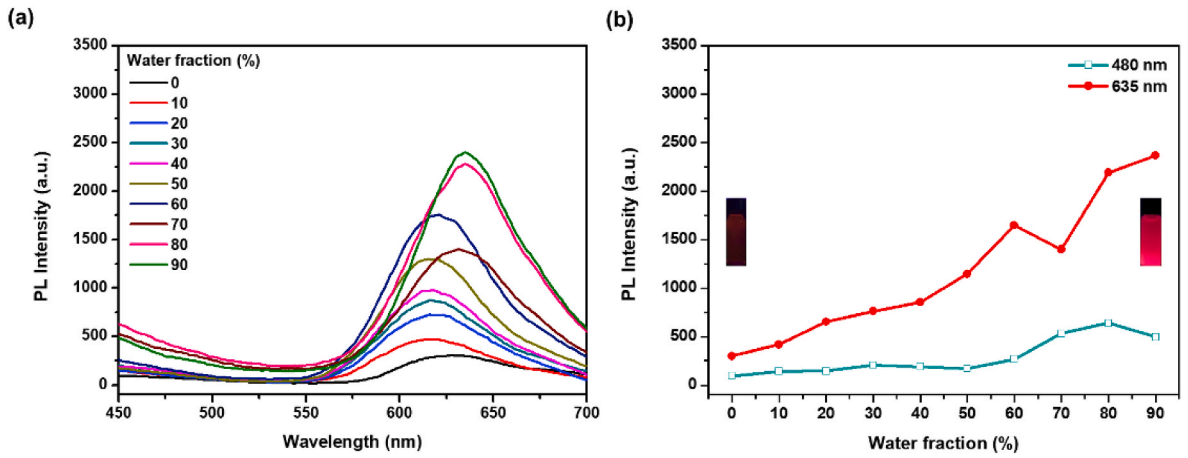

Fig. 1. (a) PL spectra of **TPE-MC-P** and (b) PL intensities at 480 nm and 635 nm of **TPE-MC-P** in THF/H_2O solutions (50 μM) with different water fractions upon UV exposure, λex = 365 nm. *Insets*: Photo-images of photoluminescence color changes at 0 and 90% H_2O. (λ_{ex} = 365 nm).

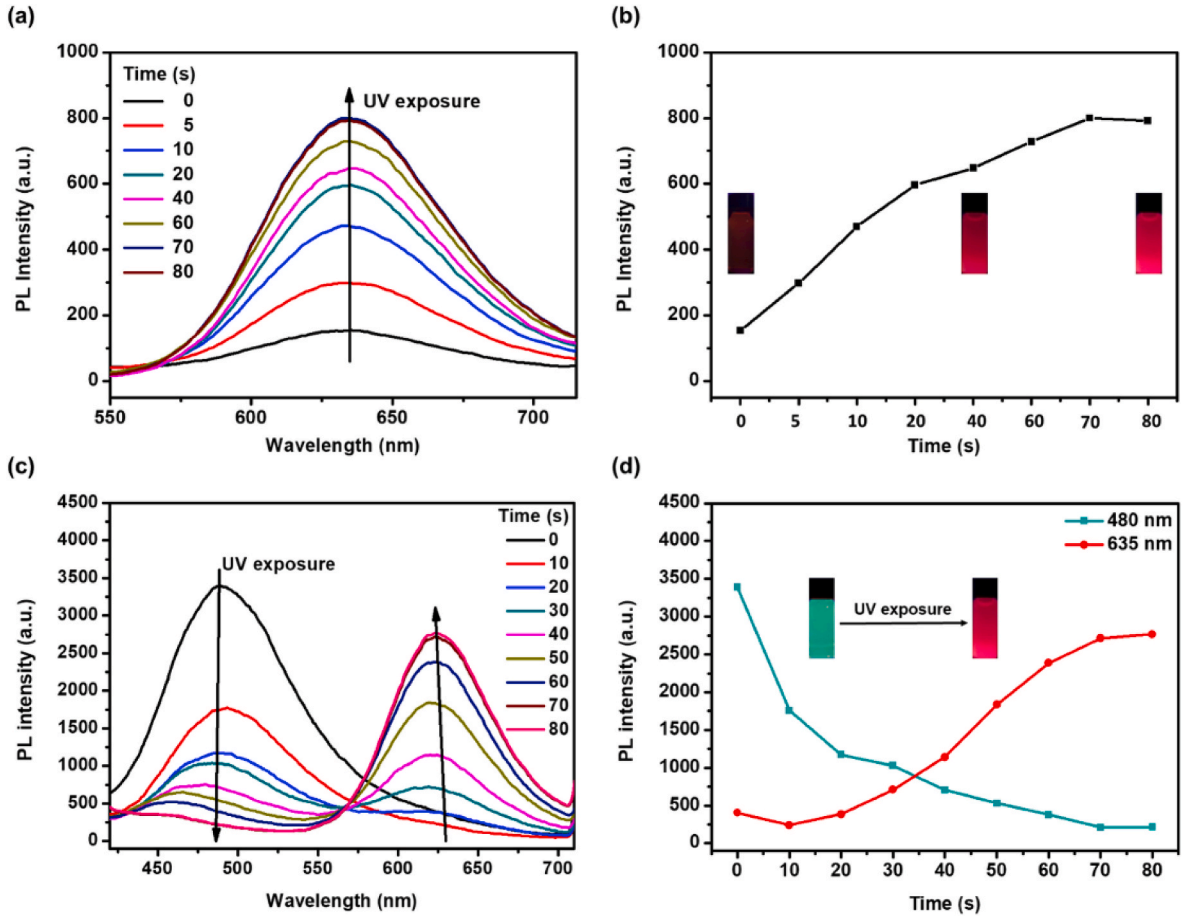

Fig. 2. Time-dependent (a) PL spectra and (b) PL intensity at 635 nm of **MC-P**; (c) PL spectra and (d) respective PL intensities at 480 nm and 635 nm of **TPE-MC-P** in THF/H_2O (10/90 vol) solutions (50 μM) upon UV exposure. *Insets*: Photo-images of PL color changes before and after UV exposure. (λ_{ex} = 365 nm).

fluorophoric **TPE-SP-P** (with close SP form), which could be photo-switchable by UV exposure to become a bi-fluorophoric sensor material (**TPE-MC-P**) containing TPE and merocyanine units with respective AIE and AIEE behaviors. Since TPE unit behaves as an energy donor and merocyanine unit acts as an acceptor, the ratiometric FRET-ON emission of bi-fluorophoric sensor material (TPE-MC-P) was observed in THF/H_2O (10/90) solution. Thus, the FRET sensor with a proper probe design can be utilized to analyze environmental and biological contaminations, and thus to show high selectivity and sensitivity towards lead ion detection.

2. Results and discussion

2.1. Water effects on AIE and FRET behaviors

Bi-fluorophoric compound **TPE-MC-P** was developed as a FRET

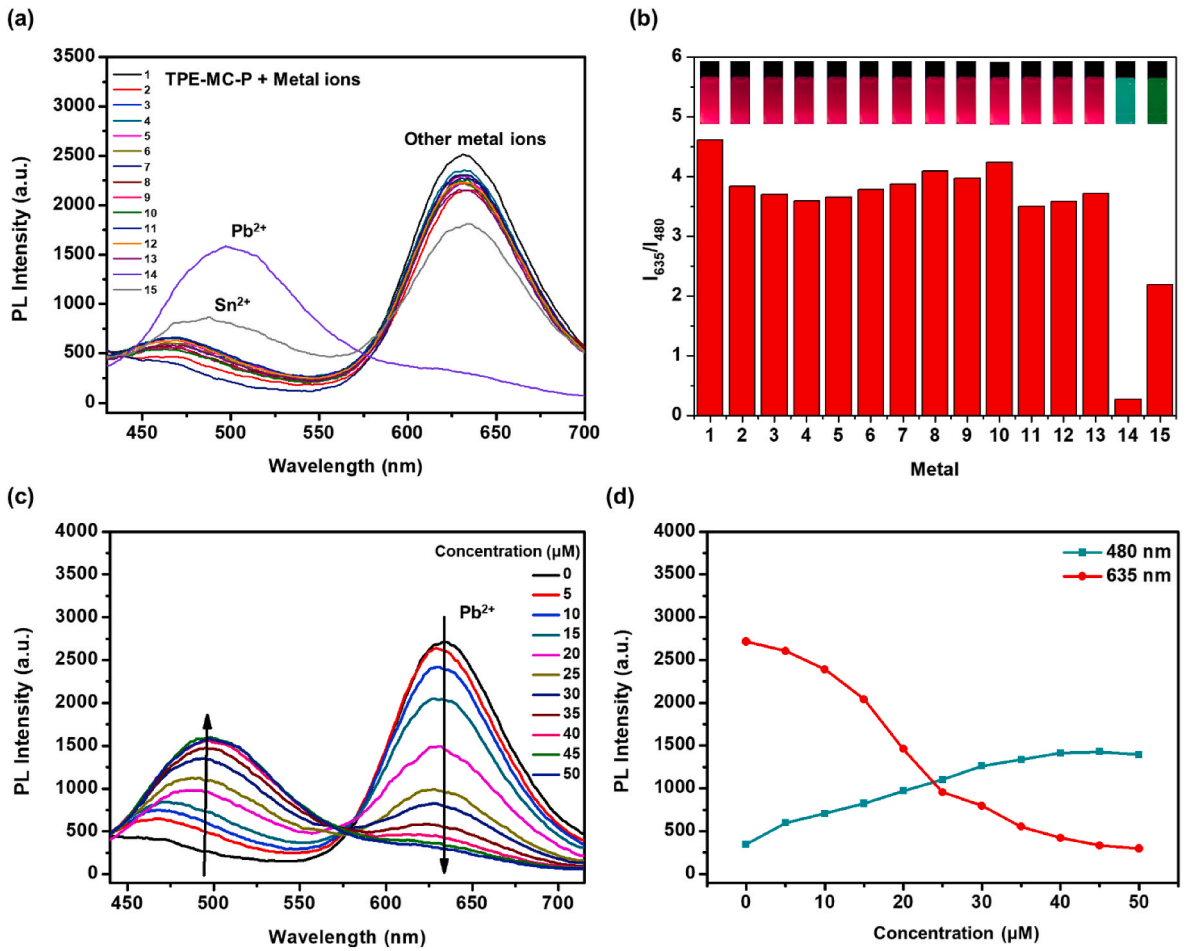

Fig. 3. (a) PL spectra of **TPE-MC-P** in THF/water (10/90 vol) solutions (50 μM) mixed with 50 μM of different metal ions and (b) relative PL ratios of **TPE-MC-P** upon the addition of various metal ions: (1) **TPE-MC-P**, (2) Al^{3+}, (3) Fe^{3+}, (4) Ca^{2+}, (5) Cd^{2+}, (6) Fe^{2+}, (7) Hg^{2+}, (8) Na^{+}, (9) Ni^{2+}, (10) K^{+}, (11) Cu^{2+}, (12) Zn^{2+}, (13) Mg^{2+}, (14) Pb^{2+} and (15) Sn^{2+}. (c) PL spectra of **TPE-MC-P** and (d) relative PL intensities of **TPE-MC-P** (50 μM) titrated with various concentrations of Pb^{2+}. *Insets*: Photo-images of photoluminescence color changes before and after mixing with different metal ions. (λ_{ex} = 365 nm).

sensor materials in this study, so mono-fluorophoric compounds **TPE-OH** and **MC-P** (see Scheme 1 and Schemes S1–S3) were designed to study their AIE behaviors in THF/H_2O solutions (with different water contents) as well as to compare the contributions of TPE unit as an energy donor and merocyanine (MC) unit as an acceptor. In order to explore the AIE and FRET behaviors, all UV–visible and photoluminescence (PL) properties of our fluorophoric materials containing TPE and/or MC units were investigated firstly, including mono-fluorophoric compounds **TPE-OH** and **MC-P** along with bi-fluorophoric compound **TPE-MC-P** and analogous mixture **TPE-OH/MC-P** (i.e., **TPE-OH**:**MC-P** = 1:1 M ratio). The UV–visible spectra of compounds **TPE-OH**, **MC-P, TPE-MC-P** and **TPE-OH/MC-P** in THF/H_2O (10/90 vol) solutions with the best PL properties are illustrated in Fig. S10. As shown in Fig. S11a and Fig. S11b, mono-fluorophoric compound **TPE-OH** has a regular AIE behavior with strong blue-green emissions at 480 nm with high water fractions (≥70% H_2O) and reaches the highest PL emission at 90% H_2O. On the other hand, mono-fluorophoric compound **MC-P** as an energy acceptor was found to have the largest absorption peak at 480 nm in Fig. S12, which matched with the emission wavelength of **TPE-OH** as a donor. The overlap between **TPE-OH** emission and **MC-P** absorption is well performed in our design strategy for an efficient FRET process in photo-switchable materials. As shown in Fig. 1a and Fig. 1b, the AIE phenomena of **TPE-MC-P** in THF/H_2O solutions reveal continuous growths of red PL emissions by increasing water contents (except 70% H_2O due to the AIEE behavior of MC unit), and the highest red PL emission at 635 nm was observed at 90% water fraction, where the blue-green TPE emissions at 480 nm of **TPE-MC-P** is weaker than that of **TPE-OH** owing to the FRET process of the energy transfer from TPE donor to MC acceptor. In the meanwhile, **MC-P** in THF/H_2O solutions exhibited AIEE behavior by increasing water contents in Fig. S11c and Fig. S11d, in which red PL emission reached the highest intensity at 60% H_2O. Therefore, the reduction of red emission at 635 nm for **TPE-MC-P** with 70% H_2O in Fig. 1b was mainly induced by AIEE behavior of **MC-P**, and thus to regain higher red emissions at water fractions ≥80% and to reach the maximum red emission for **TPE-MC-P** at 90% H_2O were offset by AIE effects of TPE donor along with FRET processes between TPE donor and MC acceptor. Accordingly, the highest red PL emission and the best FRET process of **TPE-MC-P** at 90% H_2O was chosen for sensor detection of metal ions and related applications in this report thereafter. In addition, the AIE experiments of mono-fluorophoric **TPE-SP-P** (with close SP form) in THF/H_2O solutions (with different water contents) were also carried out to demonstrate its AIE behavior in Fig. S11e and Fig. S11f similar to that of model compound **TPE-OH**.

Compared with **TPE-MC-P**, analogous mixture **TPE-OH/MC-P** was prepared by mixing compounds **TPE-OH** and **MC-P** with 1:1 M ratio to further study the results and feasibilities of our FRET sensor material **TPE-MC-P**. Among all fluorescent compounds **MC-P**, **TPE-MC-P** and mixture **TPE-OH/MC-P**, the highest red PL emission of **TPE-MC-P** was acquired as shown in Fig. S13, which also confirmed the better energy transfer of FRET in **TPE-MC-P** than that in mixture **TPE-OH/MC-P**. The PL quantum yield (QY) values of **TPE-OH**, **MC-P** and **TPE-MC-P** in THF/

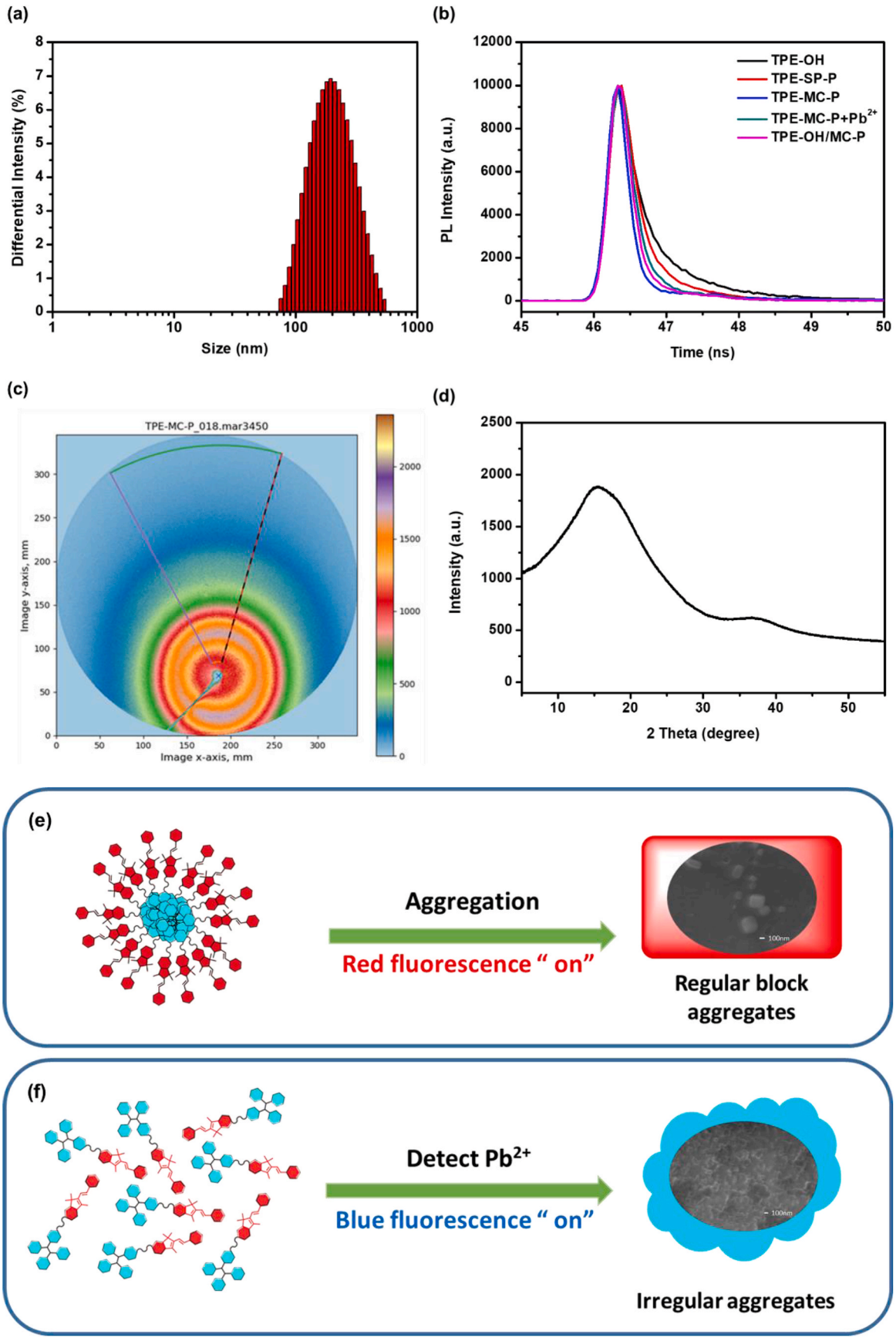

Fig. 4. (a) Dynamic light scattering (DLS) analysis of **TPE-MC-P** and (b) TRPL spectra of related compounds (λ_{ex} = 375 nm). Powders XRD patterns of **TPE-MC-P** (c) 2D, (d) 1D spectra. Cartoon representations of (e) aggregation of **TPE-MC-P** and (f) **TPE-MC-P** coordinated with Pb^{2+}. *Insets*: Scanning electron microscope (SEM) images of acquired nanoparticles from their THF/H_2O (10/90 vol) solutions (50 μM) before and after detections.

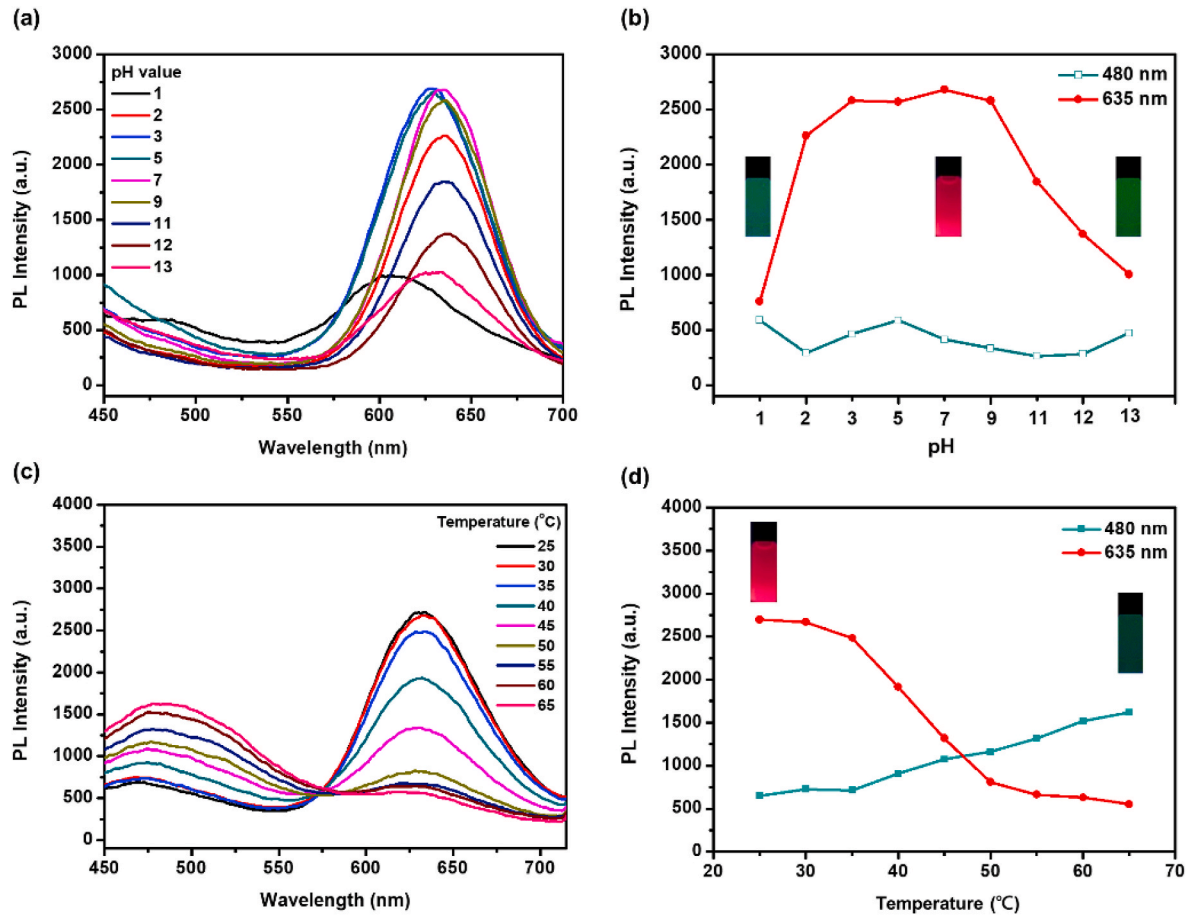

Fig. 5. (a) PL spectra of **TPE-MC-P** and (b) relative PL intensities of **TPE-MC-P** in THF/water (10/90 vol) solutions (50 μM) at 480 and 635 nm with different pH values (pH1 - pH13). (c) PL spectra of **TPE-MC-P** and (d) relative PL intensities of **TPE-MC-P** in THF/water (10/90) solutions (50 μM) at 480 and 635 nm upon heating (25–65 °C).

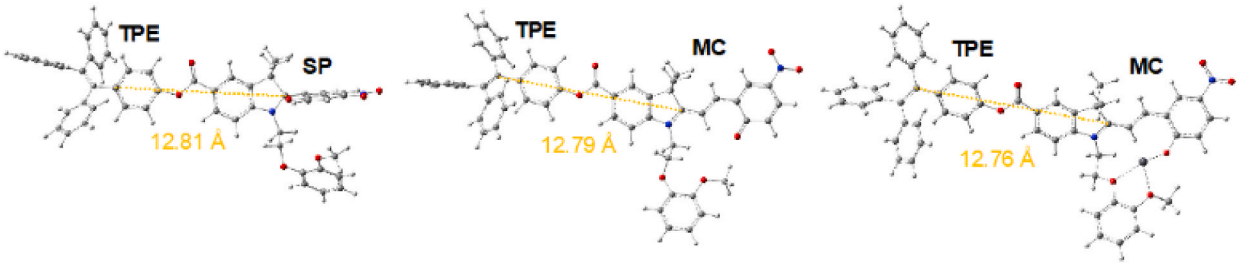

Fig. 6. Computed optimized structures for **TPE-SP-P**, **TPE-MC-P** and **TPE-MC-P** + Pb^{2+}. The distance between TPE and SP/MC units is marked in orange color.

H_2O (10/90 vol) solutions were measured in contrast to known fluorescent standards of "9,10-diphenylanthracene" with QY = 100% (λ_{ex} = 350 nm) and "rhodamine 6G" with QY = 95% (λ_{ex} = 488 nm). The fluorescence quantum yields of all products are summarized in Table S1.

The close-form of the non-emissive **SP-P** (the SP unit) can be transformed into the open-form of the red emissive **MC-P** (the MC unit) upon UV exposure (λ = 365 nm, according to the UV–visible spectra of compound **SP-P** in THF/H_2O (10/90 vol) solutions as shown in Fig. S14), which can be confirmed by the red emission of MC unit at 580–700 nm with different UV exposure time from 0 to 80 s in Fig. 2a and Fig. 2b. Since the **MC-P** saturated red emission can be observed upon 80 s of UV exposure, the exposure time of 80 s will be chosen afterward to receive the stable **MC-P** open-form in this study. Hence, the mono-fluorophoric **TPE-SP-P** can be photo-switched to a novel bi-fluorophoric **TPE-MC-P** upon UV exposure attributed to the red emissive MC unit as the energy acceptor for the Förster resonance energy transfer (FRET) process in Fig. 2c and d. Due to the FRET process, the considerable overlap of TPE donor emission to MC acceptor absorption in Fig. S12. The emission energy transferred from donor to acceptor improves the FRET efficiency of red emission in bi-fluorophoric **TPE-MC-P**. The blue-emission intensity of TPE donor at 480 nm was much reduced (ca. 10% left) in Fig. 2d after UV exposure, and the red emission of MC acceptor in **TPE-MC-P** was greatly enhanced ca. 4.2 times higher than that of MC unit alone in Fig. 2b after UV exposure. In general, the largely decreased blue-emission of TPE donor in **TPE-MC-P** after UV exposure is mainly because of the energy transfer given away via the FRET process, which is also confirmed by the theoretical study. In addition, the reversible changes of isomeric structures between **TPE-SP-P** (the close-form) and **TPE-MC-P** (the open-form) could be achieved by repeated UV irradiations (at 365 nm) and visible light, respectively,

Table 1
Absorption spectra computed at TD-M06-2X/6 31G(d)+SDD[Pb]//B3LYP/SDD.

Compounds	λ (Oscillator strength)	Electronic transition
TPE-SP-P	251 (0.32)	HOMO–13 → LUMO (62%)
	218 (0.20)	HOMO–4 → LUMO+1 (20%)
		HOMO–13 → LUMO+1 (44%)
		HOMO–17 → LUMO (27%)
TPE-MC-P	475 (1.03)	HOMO–1 → LUMO (92%)
	330 (0.32)	HOMO–4 → LUMO (52%)
	302 (0.37)	HOMO–3 → LUMO (12%)
		HOMO–1 → LUMO+2 (61%)
		HOMO–1 → LUMO+1 (24%)
TPE-MC-P + Pb^{2+}	391 (0.23)	HOMO–11 → LUMO (40%)
		HOMO–8 → LUMO (32%)

'Only absorptions involving excitations of the SP/MC units are listed. See SI for the full list of absorption peaks. Absorption wavelengths (λ) are given in nm, and only transitions with oscillator strengths (values in parenthesis) > 0.2 are listed.

which could be reversibly converted to each other for several times as shown in Fig. S15.

2.2. Metal ion detections by TPE-MC-P

Interestingly, both mono-fluorophoric **MC-P** and bi-fluorophoric **TPE-MC-P** (open-form) are not only photochromic structural isomers of corresponding **SP-P** and **TPE-SP-P** upon UV irradiation (at 365 nm), but also sensitive sensing materials toward metal ions. Firstly, the experiments of metal ion detection were conducted by mixing mono-fluorophoric **MC-P** in THF/H_2O (10/90 vol) solutions (50 μM) with 1.0 equivalent of various metal ions, including Al^{3+}, Fe^{3+}, Ca^{2+}, Fe^{2+}, Cd^{2+}, Mg^{2+}, Hg^{2+}, Ni^{2+}, Zn^{2+}, Na^{+}, K^{+}, Cu^{2+} and Pb^{2+}. Among all mentioned metal ions, lead ion (Pb^{2+}) as the only analyte could be detected by mono-fluorophoric sensor **MC-P** as illustrated in Fig. S16a and Fig. S16b. In comparison with the sensor selectivity of mono-fluorophoric **MC-P** with the complete probe (i.e., MC unit plus 1,2-dialkoxybenzene pendant group, see Scheme S2) toward lead ion (Pb^{2+}) over the other mentioned metal ions, a model compound **MC-CH$_3$** with the partial probe (i.e., without 1,2-dialkoxybenzene pendant group, see Scheme S3) was synthesized. As demonstrated in Fig. S16c and Fig. S16d, **MC-CH$_3$** showed a much poor metal ion sensitivity and a different selectivity toward Cu^{2+} (rather than **MC-P** toward Pb^{2+}). When mono-fluorophoric **MC-P** captured Pb^{2+}, the red fluorescence would be quenched, indicating that **MC-P** had the favorable selectivity and sensitivity toward lead ion as illustrated in Fig. S16a and Fig. S16b. Next, PL experiments of **MC-P** titrated with different concentrations of lead (II) ion was performed to draw out the Job's plot to estimate the binding ratio of mono-fluorophoric sensor **MC-P** with analyte Pb^{2+}. As shown in Fig. S17a and Fig. S17b, lead ion was gradually added to THF/H_2O (10/90 vol) solutions of **MC-P**, and thus to induce the gradual decreased PL emissions of **MC-P** at 635 nm upon the addition of Pb^{2+}. In addition, when **MC-P** was titrated with different mole fractions of lead ions, the Job's plot was proceeded by drawing out the equivalent of analyte Pb^{2+} with the maximum point in Fig. S18a, which could verify the binding ratio of 1:1 for **MC-P** complexed with lead (II) ion. Moreover, a possible binding structure of **MC-P** + Pb^{2+} in Fig. S18b illustrates that lone-pair electrons of phenolic oxygen and neighboring oxygens (from ether linkages) in **MC-P** could be chelated with the lead ion to eliminate the function of energy acceptor in **MC** via its coordination with Pb^{2+}.

In contrast to mono-fluorophoric **MC-P**, a better limit of detection (LOD) toward lead ion (Pb^{2+}) sensing could be acquired by bi-fluorophoric **TPE-MC-P** due to its ratiometric PL emission and FRET behavior. As revealed in Fig. 3a and Fig. 3b, a similar sensing behavior of bi-fluorophoric **TPE-MC-P** toward lead (II) ion was found. With sequential increments of lead (II) ion concentrations, the regained blue-green TPE donor emissions at 480 nm and the reduced red MC acceptor emissions at 635 nm were observed in Fig. 3c and d because of the FRET-OFF processes induced by the coordination of lead ion with **TPE-MC-P**. Normally, it is easier for human eyes to observe the blue-green fluorescence among all emission colors. However, the appreciable spectral overlap as well as the suitable distance between TPE donor and MC acceptor units in **TPE-MC-P** sensor engendered an efficient FRET process from TPE to MC unit, which resulted in a much stronger red MC emission as shown in Fig. 3d, where the insets of PL photo-images demonstrate the changes before and after mixing with Pb^{2+} ion (λex = 365 nm).As reported by the World Health Organization (WHO), the maximum permissible limit of lead (II) ion concentration in drinking water is 4.8 μM. Henceforth, to determine the sensitivities of **TPE-MC-P** and **MC-P** toward analyte Pb^{2+} based on the 3σ/k method [24], the best LOD of 0.27 μM was achieved by **TPE-MC-P** in this study, while the LOD of 1.43 μM for the detection of Pb^{2+} by **MC-P** is demonstrated in Fig. S19. Compared with some other sensor results [3,14,57] towards lead ion (Pb^{2+}) detection shown in Table S2, the lowest LOD value (0.27 μM) and the shortest detection time (30 s) of **TPE-MC-P** has demonstrated the excellent sensor capability in this report. Accordingly, it is worth noting that the color change from the red to blue-green PL emissions via the FRET-OFF process would be beneficial as a novel FRET sensor material due to the ratiometric PL detection of lead (II) ions by bi-fluorophoric **TPE-MC-P**, which would be more sensitive than a single red emission quenching process by mono-fluorophoric **MC-P**.

2.3. DLS, XRD and TRPL results

To realize the aggregation sizes of our studied materials, dynamic light scattering (DLS) experiments were carried out to achieve the average diameters of all compounds (i.e., **TPE-OH**, **SP-P**, **MC-P**, **TPE-SP-P**, **TPE-MC-P**) and its lead-coordinated derivative (i.e., **TPE-MC-P** + Pb^{2+}), and their particle size distributions are illustrated in Fig. 4a and Fig. S20 along with Table S3. As shown in the inset of Fig. S20, the SEM morphology of **TPE-OH** (50 μM) was prone to form spherical aggregates obtained from THF/H_2O (10/90 vol) solution, which was matched with the particle size around 265 nm in its DLS measurement. After UV exposure, both **MC-P** (d = 251 nm) and **TPE-MC-P** (d = 175 nm) in open-form have shown average sizes larger than the respective average sizes of their analogous close-form derivatives **SP-P** (d = 230 nm) and **TPE-SP-P** (d = 142 nm) before UV exposure, which could be attributed to the longer conjugated MC structure in both **MC-P** and **TPE-MC-P** after UV exposure to induce extended π-π conjugations and aggregations. It must be emphasized that the SEM morphologies of **SP-P** and **MC-P** are different from those of **TPE-SP-P** and **TPE-MC-P**, respectively, because the aggregation effects of SP and MC units were weaker than the TPE unit. The SEM morphologies of **SP-P** and **MC-P** were irregular, but in case of **TPE-SP-P** and **TPE-MC-P** the morphologies were regular block. Finally, the coordination of Pb^{2+} to **TPE-MC-P** (d = 180 nm) preceded its morphological change from regular block to irregular as demonstrated in Fig. 4e and f.

As shown in Fig. S21, we studied XRD patterns of **TPE-SP-P** derivatives, including **TPE-OH**, **SP-P**, **MC-P** and **TPE-SP-P** powders. Thus, the X-ray diffraction (XRD) experiments of **TPE-MC-P** powders were performed (Fig. 4c and d). **TPE-SP-P** was difficult to crystallize because of its high molecular weight (MW = 863), which made it difficult to verify the molecular structure and packing of **TPE-SP-P**. In the wide-angle region, the relatively weak and broad diffraction peaks in solid powders of **TPE-SP-P** at 2θ = 37.1 and 15.7 corresponding to d-spacing values of 2.08 and 4.83 Å, respectively. In addition, as **TPE-SP-P** changed to **TPE-MC-P** after UV exposure, the XRD results did not show obvious variations in molecular arrangements regardless of their structural changes.

To further verify the FRET process from the blue-green emissive TPE donor to the red emissive MC acceptor, the average lifetime values of the TPE (donor) emission in **TPE-OH**, **TPE-SP-P**, **TPE-MC-P**, **TPE-OH/MC-P** (mixture of **TPE-OH** and **MC-P** in 1:1 M ratio) and its lead-coordinated derivative (i.e., **TPE-MC-P** + Pb^{2+}) were investigated by time-resolved photoluminescence (TRPL) spectra (excited at λ_{ex} = 375 nm and

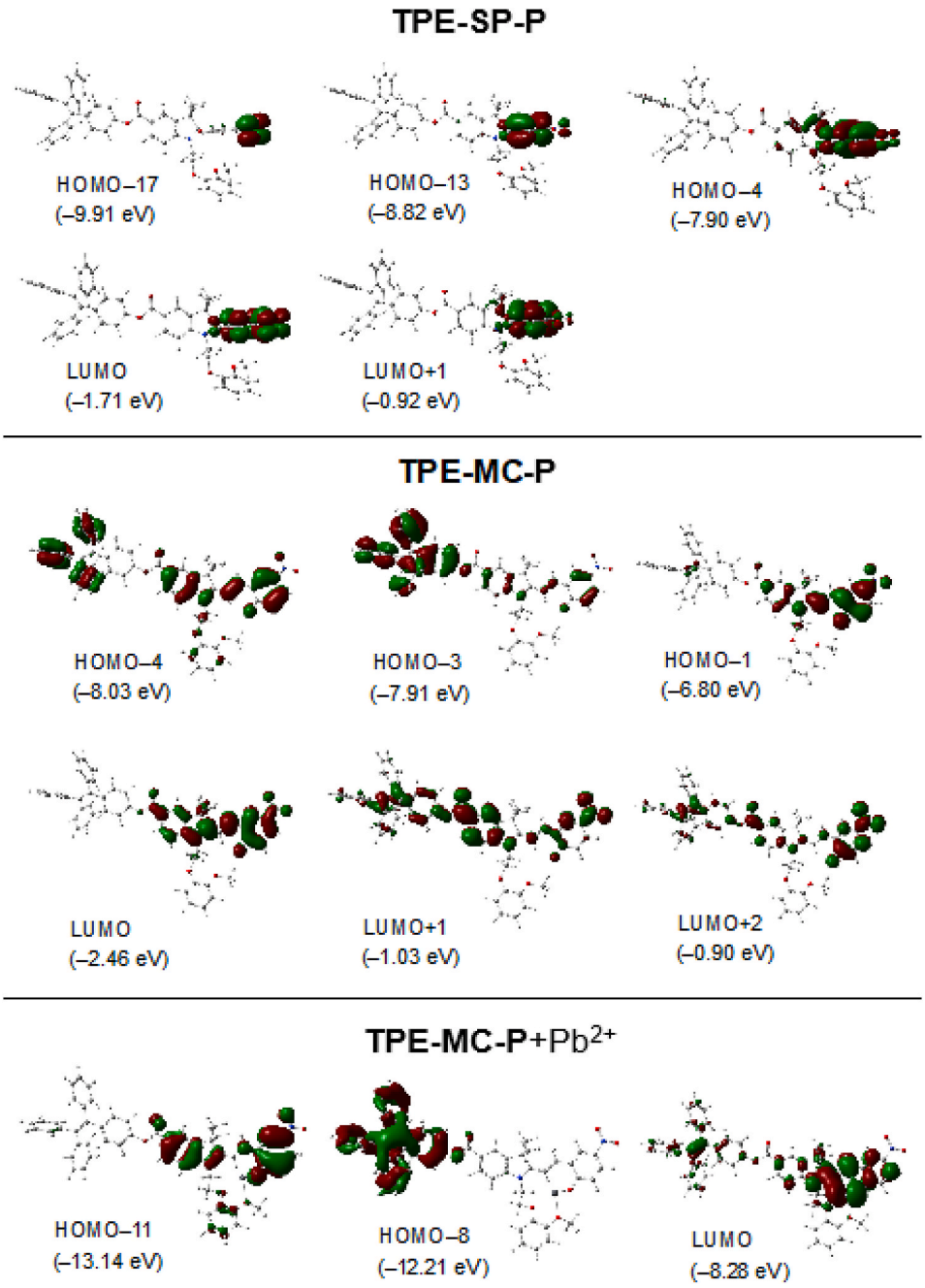

Fig. 7. Molecular orbitals involved in SP/MC excitation of **TPE-SP-P**, **TPE-MC-P** and **TPE-MC-P** + Pb^{2+}. The orbital energies were computed at M06-2X/6-31G(d)+SDD[Pb]//B3LYP/SDD.

monitored at λ_{em} = 480 nm of TPE emission) and illustrated in Fig. 4b and Table S2. In comparison with lifetime values of 7.65, 5.10 and 1.02 ns in **TPE-OH**, **TPE-SP-P** and **TPE-OH/MC-P**, the most efficient energy transfer from the TPE donor to MC acceptor in **TPE-MC-P** was verified by its shortest lifetime of 0.44 ns in Table S2. Since the best FRET process was acquired by bi-fluorophoric **TPE-MC-P**, we can calculate the FRET efficiency (E_{FRET}) of **TPE-MC-P** by the following formula:

$$E_{FRET} = 1 - \frac{\tau_{DA}}{\tau_D} = \left(1 - \frac{\tau_{(TPE-MC-P)}}{\tau_{(TPE-SP-P)}}\right) = \left(1 - \frac{0.44}{5.10}\right) \fallingdotseq 91\%$$

where τ_{DA} and τ_D denote the fluorescence lifetime values of the bi-fluorophoric **TPE-MC-P** (i.e., FRET system) and mono-fluorophoric **TPE-SP-P** (i.e., without energy acceptor), respectively. Hence, the corresponding E_{FRET} value of 91 % in **TPE-MC-P** was acquired owing to the prominent energy transfer between donor and acceptor. In contrast to the lifetime of **TPE-MC-P** (0.44 ns), **TPE-MC-P** + Pb^{2+} had a longer lifetime of 1.48 ns, which demonstrated the induced FRET-OFF process after the complexation of Pb^{2+} with **TPE-MC-P**. As a result, the significant FRET-OFF process of lead-coordinated derivative (i.e., **TPE-MC-P** + Pb^{2+}) took place and the blue-green donor emission was restored (at λ_{em} = 480 nm) to regain the longer lifetime of TPE (donor) emission. Therefore, the most effective FRET process and the significant ratiometric PL behavior of the blue-green TPE donor emission (at 480 nm) and red MC acceptor emission (at 635 nm) have led to the highly potential FRET sensor applications of **TPE-MC-P** toward Pb^{2+} detection.

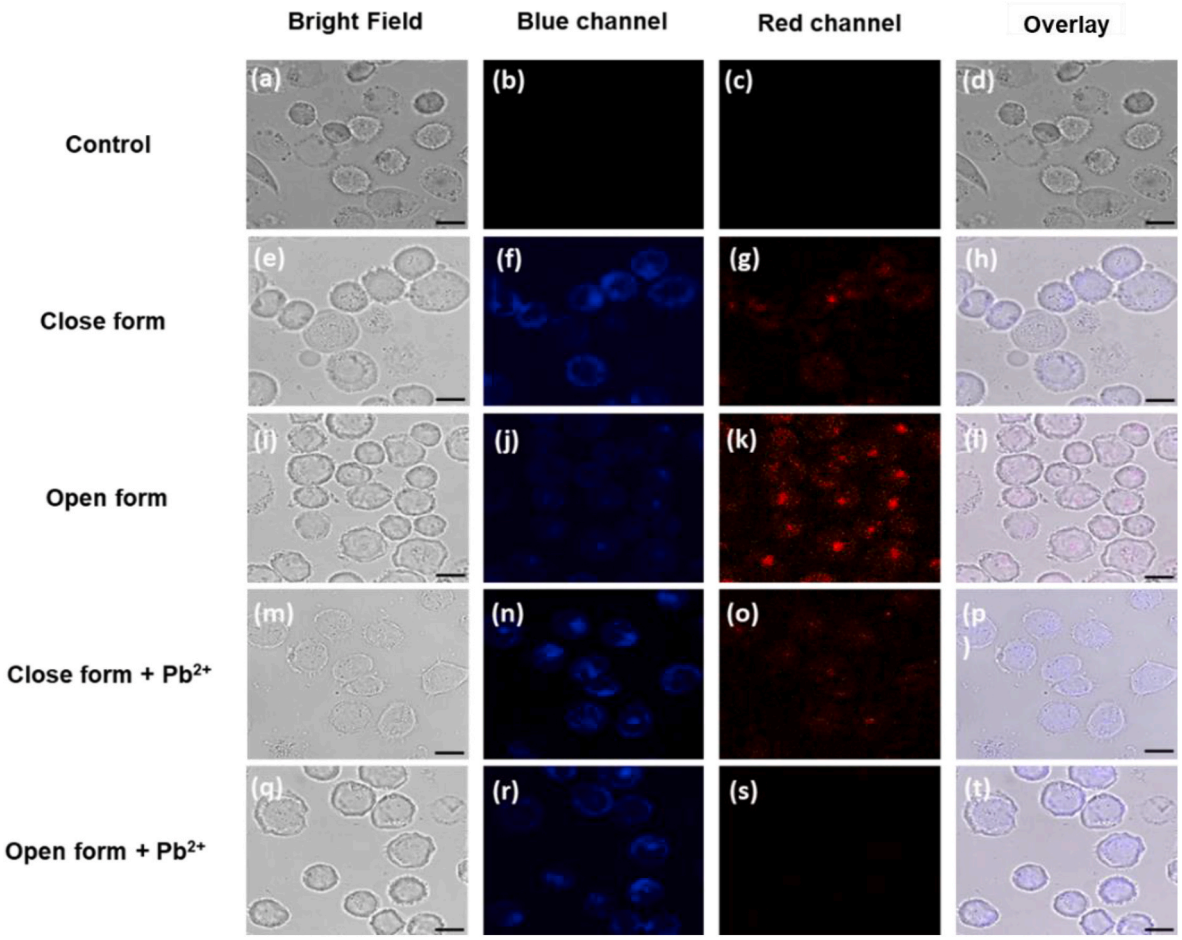

Fig. 8. Confocal PL images of HeLa all followed by incubation for 30 min. (a–d) Control experiments of HeLa. (e–h) Cells were treated with **TPE-SP-P**. (i–l) Cells were treated with sensor **TPE-MC-P**. (m–p) Cells were treated with **TPE-SP-P** and Pb^{2+} ion. (q–t) Cells were treated with sensor **TPE-MC-P** and Pb^{2+} ion. The concentrations of sensor along with Pb^{2+} ions is 10 μM. Scale bars = 10 μm.

2.4. pH and temperature effects on FRET behavior

Under severe conditions and environments, less fluorescence responses to acidity/basicity and temperature are expected to possess these important features for general sensor applications. For the open form of **TPE-MC-P**, the fluorescence intensity changed dramatically in responses to the changes of pH values in Fig. 5. Under various acid and base environments (pH = 1–2 and 9–13), the intensities of red fluorescent at 635 nm diminished due to the protonation/deprotonation in **TPE-MC-P** (Fig. 5a). Interestingly, the blue-green TPE donor emission could not be restored (see Fig. 5b), even if the FRET-OFF process occurred (by the quenching of red emission at 635 nm). However, as the pH value was maintained at pH = 3–9, the strong and stable red fluorescence behavior (i.e., FRET-ON) was still observed in **TPE-MC-P**, showing the practicality of our sensor over a wide range of pH values (3–9).

Less temperature effects on the MC probe with reversible isomerization reaction are expected for useful sensor applications. Therefore, to observe the changes of fluorescence emissions at different temperatures, the PL spectra in the open form of **TPE-MC-P** (under UV irradiation for 80 s) were acquired in Fig. 5c among 25–65 °C, where the relative changes of PL intensity between TPE and MC units (at 480 nm and 635 nm, respectively) is demonstrated in Fig. 5d. Interestingly, the blue-green TPE emission of **TPE-MC-P** at 480 nm was gradually recovered by heating above 45 °C, and the red MC emission at 635 nm was gradually decreased, which was induced by the FRTE-OFF process due to the transformation of the MC to SP form by heating [24]. Though the temperature effects on the FRET behavior were observed at high temperatures, the red MC emission at 635 nm and the FRET-ON process of **TPE-MC-P** upon UV irradiation can be maintained at temperatures below 45 °C and thus to be utilized for further sensor applications.

2.5. Theoretical study

Theoretical calculations were computed for **TPE-SP-P, TPE-MC-P, TPE-MC-P** + Pb^{2+}, **TPE-SP-CH_3** and **TPE-MC-CH_3** in order to investigate the mechanism of FRET switching. All structures were optimized at B3LYP/SDD. The absorption spectra of these compounds were computed using the time dependent density functional theory (TD-DFT) approach at M06-2X/6-31G(d), with the SDD basis set used for Pb^{2+} (denoted as 6-31G(d)+SDD[Pb^{2+}] in the rest of the text). All the calculations were performed in the gas phase using Gaussian 16 program.

Optimized structures show that the distance between TPE and SP/MC unit is ~12.8 Å in Fig. 6, within the range of required donor-acceptor distance (1–10 nm) for the FRET process. The computed absorption spectra are listed in Table 1 and Fig. S22 to Fig. S27. For **TPE-MC-P**, the excitation on MC unit (See Fig. 7 for the molecular orbitals involved in the excitation) gives a strong absorption at 475 nm, matching the blue-green TPE emission at 480 nm in experiments leading to an effective TPE donor to MC acceptor of the FRET process. However, the excitation on SP unit results in an absorption of 251 nm, and the FRET process of TPE to SP unit does not occur. The coordination of Pb^{2+} to MC unit increase

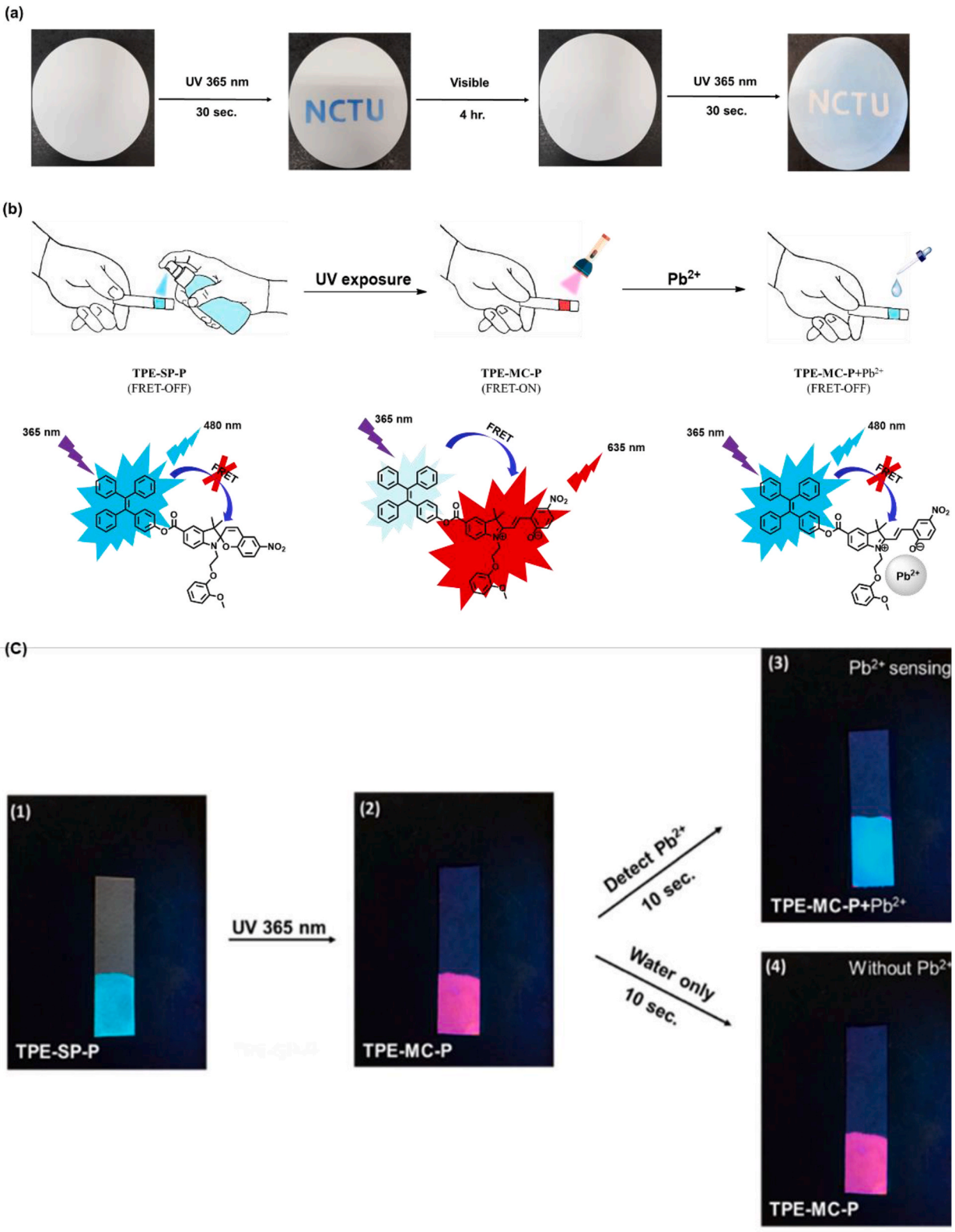

Fig. 9. (a) After respective UV–visible light exposures of filter paper containing **TPE-SP-P**. (b) Preparation process of test paper **TPE-MC-P** and their responsive PL emissions. (c) PL images of primitive test paper **TPE-SP-P** (1) before UV exposure, (2) converted to **TPE-MC-P** after UV exposure and (3) test paper **TPE-MC-P** detected with lead-contaminated domestic water (top image, i.e., **TPE-MC-P** + Pb^{2+}) and (4) lead-free domestic water (bottom image, i.e., **TPE-MC-P**).

the HOMO-LUMO energy gap from 4.34 eV (HOMO–1 → LUMO in **TPE-MC-P**) to 4.86 eV (HOMO–11 → LUMO in **TPE-MC-P** + Pb^{2+}), resulting in a shorter absorption wavelength (391 nm) for the MC excitation, where the FRET process was absent from the TPE to MC unit. The same FRET-OFF/ON mechanism is also observed in the case of **TPE-SP-CH$_3$** and **TPE-MC-CH$_3$**. The energy transfer was found from TPE to MC unit,

but it was not observed from TPE to SP unit in Table 1 and Fig. 7.

2.6. Cell culture and confocal fluorescence imaging of TPE-MC in living cells

Since lead ion is highly toxic to biological systems and environments, to detect Pb^{2+} by selective sensor materials becomes an important issue nowadays. We conducted a confocal fluorescence imaging detection on living cells to further study the effect of sensor **TPE-MC-P** with the strongest FRET process, where the cytotoxicities of the close and open forms of sensor **TPE-MC-P** were assessed by a standard MTS assay using HeLa cells. As shown in Fig. S28, when the cells were treated with 0–25 μM **TPE-SP-P** and **TPE-MC-P** for 24 h, the cell viabilities were higher than 80%, which indicates that both close and open forms of **TPE-SP-P** and **TPE-MC-P** had low cytotoxicities.

With the FRET merits of bi-fluorophoric sensor, **TPE-MC-P** can be applied to observe the bio-imaging of HeLa cells by confocal fluorescence microscopy. In addition to control experiments (in Fig. 8a to Fig. 8d), the related confocal bio-images of **TPE-SP-P** and sensor **TPE-MC-P** toward Pb^{2+} detection are shown in Fig. 8. In general, the close form of sensor **TPE-SP-P** revealed a strong blue channel PL emission in Fig. 8f, while the open form of sensor **TPE-MC-P** had a strong red channel of PL emission in Fig. 8k and its blue channel PL emission in Fig. 8j decreased due to the FRET-ON process. As shown in Fig. 8m to p and Fig. 8q to t, the close form of sensor **TPE-SP-P** did not show any obvious PL changes after the addition of Pb^{2+} ion. Besides, the open form of sensor **TPE-MC-P** revealed obvious color changes of PL emission from red to blue after the addition of Pb^{2+} ion in Fig. 8q to t due to FRET-OFF processes. Based on above experiments, these results indicated that the open form of sensor **TPE-MC-P** could be utilized for bio-imaging applications to lead detections in living cells.

2.7. Application of rapid test papers to detect lead ion

As an ion sensor material, it is an important scientific goal to emphasize economic, speedy, and accurate detection in modern life. In this study, we first dissolved TPE-SP-P in THF to prepare a sensor solution, then spray the solution onto the paper strip. Finally, the test paper was dried and exposed to UV irradiation (365 nm) for 30 s in Fig. 9a. The close form of TPE-SP-P would become the open form of TPE-MC-P upon UV exposure, which induced the color change from white to blue. After visible light exposure of test paper TPE-MC-P for 4 h, the visible characters almost disappeared, meaning that TPE-MC-P transformed back to TPE-SP-P. The reversible color changes of alternative UV–visible irradiations were proven to be repetitive for several cycles.

For the application of test paper preparation process in Fig. 9b, we simulated polluted water by.

Adding lead ion into domestic water. Therefore, the detection of lead ion in polluted domestic water by the red emission of the FRET process on the test paper containing TPE-MC-P was compared with that of pollution-free domestic water. As shown in Fig. 9c, we spray the **TPE-SP-P** solution onto the paper strip to prepare a test paper **TPE-SP-P**. After UV irradiating (365 nm) for 30 s, the close form of **TPE-SP-P** on the test paper can be converted into the open form of **TPE-MC-P** with a FRET-ON process, where the red fluorescence of the MC emission could be observed. In addition, the open form of **TPE-MC-P** toward Pb^{2+} detection to proceed the FRET-OFF process would regain its blue fluorescence of the TPE emission rapidly (ca. 30 sec). The experiment confirmed that test paper **TPE-MC-P** had a fast and accurate detection function toward Pb^{2+}. The test paper could show a quick FRET-OFF change to demonstrate competitive lead ion detection in the future.

3. Conclusion

In summary, we have developed a bi-fluorophoric AIE sensor **TPE-MC-P** containing TPE and MC fluorophores in semi-aqueous media to reveal ratiometric PL behavior between blue-green (λ_{em} = 480 nm) and red (λ_{em} = 635 nm) emissions from TPE donor and MC acceptor, respectively, which induced novel FRET-ON processes for further sensor applications. Upon UV exposure (λ = 365 nm), the close-form of non-emissive SP unit can be transformed into the open-form of red-emissive MC unit, so the bi-fluorophoric AIE sensor **TPE-MC-P** can be acquired from mono-fluorophoric **TPE-SP-P** by UV irradiation. Furthermore, theoretical calculations also confirmed the possible speculated molecular arrangements and FRET processes of **TPE-MC-P**, along with DLS and XRD measurements were studied as well. Moreover, the strongest red MC emission of **TPE-MC-P** with the best FRET process was achieved in THF/H_2O (10/90 vol) solution (50 μM), which was also verified by TRPL measurements with the shortest lifetime of 0.44 ns. Since the MC unit in mono-fluorophoric **MC-P** could be coordinated with Pb^{2+} ion in 1:1 M ratio, the quenching of red MC emission (λ_{em} = 635 nm) in **MC-P** could detect lead(II) ion with the corresponding LOD value of 1.43 μM. Comparatively, the ratiometric PL quenching of red MC acceptor emission to recover blue-green TPE donor emission occurred in the detection of Pb^{2+} by bi-fluorophoric **TPE-MC-P** via the FRET-OFF process. So far, very few AIE sensor molecules have been utilized for cation detections, so our designed **TPE-MC-P** shows more significant sensitivities and selectivities of cation detections toward lead (II) ion with the best LOD value of 0.27 μM, which is much lower than the standards of U.S. EPA, i.e., 4.8 μM. In spite of pH and temperature effects, the highest red MC unit emissions with the optimum FRET processes of **TPE-MC-P** were obtained around 25–45 °C and wide pH conditions (i.e., pH = 3–9), though higher temperatures (T > 45 °C), stronger acidic (pH < 3) and basic (pH > 10) conditions would cause the MC unit structural changes to reduce the red MC emissions, or even at higher temperatures (T > 45 °C) to recover blue-green emissions partially (or completely at T = 65 °C) induced by the close-form of **TPE-SP-P** via FRET-OFF behavior. The cell viability tests also validated the non-toxic and remarkable bio-marker of **TPE-MC-P**, so this novel FRET-OFF sensor toward lead (II) ion could be utilized for bio-imaging applications to lead detections in living cells. Finally, we also demonstrated the fast and accurate detection of Pb^{2+} by test paper **TPE-MC-P** via the FRET-OFF process.

Declaration of competing interest

The authors declare that they have no known competing financial interests or personal relationships that could have appeared to influence the work reported in this paper.

Acknowledgements

The authors are grateful for funding from the Ministry of Science and Technology, Taiwan, ROC. This work is supported by Ministry of Science and Technology, Taiwan (grant No. MOST106-2113-M-009-012-MY3, MOST107-2221-E-009-043-MY2, and MOST108-3017-F-009-004) and the Center for Emergent Functional Matter Science of National Yang Ming Chiao Tung University from The Featured Areas Research Center Program within the framework of the Higher Education Sprout Project by the Ministry of Education (MOE) in Taiwan. J. I. W. thanks the National Science Foundation (CHE-1751370) and the National Institute of General Medical Sciences (NIGMS) of the National Institute of Health (R35GM133548) for grant support, as well as computational resources provided by the HPC cluster, managed by the University of Houston and acquired through support from the NSF (MRI-1531814).

Appendix A. Supplementary data

Supplementary data to this article can be found online at https://doi.org/10.1016/j.dyepig.2021.109238.

References

[1] Dong R-E, Kang P, Xu X-L, Cai L-X, Guo Z. Cation-exchange strategy for a colorimetric paper sensor: belt-like ZnSe nanoframes toward visual determination of heavy metal ions. Sensor Actuator B 2020;312. 128013.

[2] Yang Z, Liu H, Li J, Yang K, Zhang Z, Chen F, Wang B. High-throughput metal trap: sulfhydryl-functionalized wood membrane stacks for rapid and highly efficient heavy metal ion removal. ACS Appl Mater Interfaces 2020;12:15002–11.

[3] Liu T, Wan X, Yao Y. Dual sensitive and selective sensor for Pb^{2+} and Al^{3+} with distinctive fluorescence response. Sensor Actuator B 2018;254:1094–100.

[4] Diao W, Wang G, Wang L, Zhang L, Ding S, Takarada T, Maeda M, Liang X. Opposite effects of flexible single-stranded DNA regions and rigid loops in DNAzyme on colloidal nanoparticle stability for "turn-on" plasmonic detection of lead ions. ACS Appl. Bio Mater. 2020;3:7003–10.

[5] Xu J, Xiong J, Qin Y, Li Z, Pan C, Huo Y, Zhang H. A novel quinolinyl-tetraphenylethene-based fluorescence "turn-on'' sensor for Zn^{2+} with a large Stokes shift and its applications for portable test strips and biological imaging. Mater. Chem. Front. 2020;4:3338–48.

[6] Manna M, Roy S, Bhandari S, Chattopadhyay A. A dual-emitting quantum dot complex nanoprobe for ratiometric and visual detection of Hg^{2+} and Cu^{2+} ions. J Mater Chem C 2020;8:6972–6.

[7] Ho FC, Huang YJ, Weng CC, Wu CH, Li YK, Wu JI, Lin HC. Efficient FRET approaches toward copper(II) and cyanide detections via host-guest interactions of photo-switchable [2]Pseudo-Rotaxane polymers containing naphthalimide and merocyanine moieties. ACS Appl Mater Interfaces 2020;12:53257–73.

[8] Peng D, Li I, Huang Z, Liang RP, Qiu JD, Liu J. Efficient DNA-catalyzed porphyrin metalation for fluorescent ratiometric Pb^{2+} detection. Anal Chem 2019;91:11403–8.

[9] Chen C, Chen D, Xie S, Quan H, Luo X, Guo L. Adsorption behaviors of organic micropollutants on zirconium metal-organic framework UiO-66: analysis of surface interactions. ACS Appl Mater Interfaces 2017;9:41043–54.

[10] Singh R, Xiao CC, Wei CL, Ho FC, Khang TM, Gouda C, Wu TK, Li YK, Wei KH, Lin HC. Optical-switchable energy transfer controlled by multiple-responsive turn-on fluorescence via metal-ligand and host-guest interactions in diarylethene-based [2]pseudo-rotaxane polymers. Mater. Chem. Front. 2020. https://doi.org/10.1039/D0QM00605J.

[11] Abdollahi A, Alinejad Z, Mahdavian AR. Facile and fast photosensing of polarity by stimuli-responsive materials based on spiropyran for reusable sensors: a physico-chemical study on the interactions. J Mater Chem C 2017;5:6588–600.

[12] Lin T, Su X, Wang K, Li M, Guo H, Liu L, Zou B, Zhang YM, Liu Y, Zhang SXA. An AIE fluorescent switch with multi-stimuli responsive properties and applications for quantitatively detecting pH value, sulfite anion and hydrostatic pressure. Mater. Chem. Front. 2019;3:1052–61.

[13] Chai X, Han HH, Sedgwick AC, Li N, Zang Y, James TD, Zhang J, Hu XL, Yu Y, Li Y, Wang Y, Li J, He XP, Tian H. Photochromic fluorescent probe strategy for the super-resolution imaging of biologically important biomarkers. J Am Chem Soc 2020;142:18005–13.

[14] Deshpande SS, Jachak MA, Khopkar SS, Shankarling GS. A simple substituted spiropyran acting as a photo reversible switch for the detection of lead (Pb^{2+}) ions. Sensor Actuator B 2018;258:648–56.

[15] He X, Xu W, Xu C, Ding F, Chen H, Shen J. Reversible spiropyran-based chemosensor with pH-switches and application for bioimaging in living cells, Pseudomonas aeruginosa and zebrafish. Dyes Pigments 2020;180. 108497.

[16] Kumar R, Sharma A, Singh H, Suating P, Kim HS, Sunwoo K, Shim I, Gibb BC, Kim JS. Revisiting fluorescent calixarenes: from molecular sensors to smart materials. Chem Rev 2019;119:9657–721.

[17] Khan A, Kisannagar RR, Gouda C, Gupta D, Lin HC. Highly stretchable supramolecular conductive self-healable gels for injectable adhesive and flexible sensor applications. J Mater Chem A 2020;8:19954–64.

[18] Okino K, Sakamaki D, Seki S. Dicyanomethyl radical-based near-infrared thermochromic dyes with high transparency in the visible region. ACS Materials Lett 2019;1:25–9.

[19] Yan Q, Wang S. Fusion of aggregation-induced emission and photochromics for promising photoresponsive smart materials. Mater. Chem. Front. 2020;4:3153–75.

[20] Huang W, Long Y, Yang T, Zhou Z, Qu L, Wu M, Qi X, Liu S, Chi Z, Xu J, Zhang Y. Functional polyimides based on diamine containing diarylethylene moieties and their photochromic mechanism studies. Polym Chem 2020;11:6701–7.

[21] Gossweiler GR, Brown CL, Hewage GB, Gheiler ES, Trautman WJ, Welshofer GW, Craig GW. Mechanochemically active soft robots. ACS Appl Mater Interfaces 2015;7:22431–5.

[22] Gelebart AH, Mulder DJ, Varga M, Konya A, Vantomme G, Meijer EW, Selinger RLB, Broer DJ. Making waves in a photoactive polymer film. Nature 2017;546:632–6.

[23] Li C, Iscen A, Palmer LC, Schatz GC, Stupp SI. Light-driven expansion of spiropyran hydrogels. J Am Chem Soc 2020;142:8447–53.

[24] Nhien PQ, Chou WL, Cuc TTK, Khang TM, Wu CH, Thirumalaivasan N, Hue BTB, Wu JI, Wu SP, Lin HC. Multi-stimuli responsive FRET processes of bifluorophoric AIEgens in an amphiphilic copolymer and its application to cyanide detection in aqueous media. ACS Appl Mater Interfaces 2020;12:10959–72.

[25] Zhou S, Guo S, Liu W, Yang Q, Sun H, Ding R, Qian Z, Feng H. Rational design of reversibly photochromic molecules with aggregation-induced emission by introducing photoactive thienyl and benzothienyl groups. J Mater Chem C 2020;8:13197–204.

[26] Huang G, Xia Q, Huang W, Tian J, He Z, Li BS, Tang BZ. Multiple anti-counterfeiting guarantees from a simple tetraphenylethylene derivative-high-contrasted and multi-state mechanochromism and photochromism. Angew Chem Int Ed 2019;58:17814–9.

[27] Wang S, Ma L, Liu G, Pu S. Diarylethene-based fluorescent and colorimetric chemosensor for the selective detection of Al^{3+} and CN^{-}. Dyes Pigments 2019;164:257–66.

[28] Nhien PQ, Cuc TTK, Khang TM, Wu CH, Hue BTB, Wu JI, Mansel BW, Chen HL, Lin HC. Highly efficient förster resonance energy transfer modulations of dual-AIEgens between a tetraphenylethylene donor and a merocyanine acceptor in photo-switchable [2]Rotaxanes and reversible photo-patterning applications. ACS Appl Mater Interfaces 2020;12:47921–38.

[29] Peng J, Ye K, Liu C, Sun J, Lu R. The photomechanic effects of the molecular crystals based on 5-chloro-2-(naphthalenylvinyl)benzoxazols fueled by topo-photochemical reactions. J Mater Chem C 2019;7:5433–41.

[30] Florea L, McKeon A, Diamond D, Benito-Lopez F. Spiropyran polymeric microcapillary coatings for photodetection of solvent polarity. Langmuir 2013;29:2790–7.

[31] Wan S, Zheng Y, Shen J, Yang W, Yin M. On–off–on switchable sensor: a fluorescent spiropyran responds to extreme pH conditions and its bioimaging applications. ACS Appl Mater Interfaces 2014;6:19515–9.

[32] Chen J-R, Yang D-Y. Design and synthesis of an o-hydroxyphenyl-containing spiropyran thermochromic colorant. Org Lett 2009;11:1769–72.

[33] Cuc TTK, Nhien PQ, Khang TM, Weng CC, Wu CH, Hue BTB, Li YK, Wu JI, Lin HC. Optimization of FRET behavior in photo-switchable [2]Rotaxanes containing Bi-fluorophoric naphthalimide donor and merocyanine acceptor with sensor approaches toward sulfite detection. Chem Mater 2020;32:9371–89.

[34] Hong Y, Lam JWY, Tang B-Z. Aggregation-induced emission. Chem Soc Rev 2011;40:5361–88.

[35] Yan Q, Li C, Wang S, Lin Z, Yan Q, Cao D. Visible light responsive donor-acceptor stenhouse adducts with indoline-tri/tetra-phenylethylene chromophore: synthesis, aggregation-induced emission, photochromism and solvent dependence effect. Dyes Pigments 2020;178. 108352.

[36] Huang M, Yu R, Xu K, Ye S, Kuang S, Zhu X, Wan Y. An arch-bridge-type fluorophore for bridging the gap between aggregation-caused quenching (ACQ) and aggregation-induced emission (AIE). Chem Sci 2016;7:4485–91.

[37] Luo J, Xie Z, Lam JWY, Cheng L, Chen H, Qiu C, Kwok H-S, Zhan X, Liu Y, Zhuc D, Tang B-Z. Aggregation-induced emission of 1-methyl-1,2,3,4,5-pentaphenylsilole. Chem Commun 2001:1740–1.

[38] Zheng X, Zhu W, Zhang C, Zhang Y, Zhong C, Li H, Xie G, Wang X, Yang C. Self-assembly of a highly emissive pure organic imine-based stack for electroluminescence and cell imaging. J Am Chem Soc 2019;141:4704–10.

[39] Cheng Y, Wang J, Qiu Z, Zheng X, Leung NLC, Lam JWY, Tang B-Z. Multiscale humidity visualization by vnvironmentally sensitive fluorescent molecular rotors. Adv Mater 2017;29. 1703900.

[40] Wang F, Wen J, Huang L, Huang J, Ouyang J. A highly sensitive "switch-on" fluorescent probe for protein quantification and visualization based on aggregation-induced emission. Chem Commun 2012;48:7395–7.

[41] Kwok RTK, Leung CWT, Lam JWY, Tang B-Z. Biosensing by luminogens with aggregation induced emission characteristics. Chem Soc Rev 2015;44:4228–38.

[42] Dai D, Li Z, Yang J, Wang C, Wu J-R, Wang Y, Zhang D, Yang Y-W. Supramolecular assembly-induced emission enhancement for efficient mercury(II) detection and removal. J Am Chem Soc 2019;141:4756–63.

[43] Liu P, Li B, Zheng J, Liang Q, Wu C, Huang L, Zhang P, Jia Y, Wang S. A novel N-nitrosation-based ratiometric fluorescent probe for highly selective imaging endogenous nitric oxide in living cells and zebrafish. Sensor Actuator B Chem 2021;329. 129147.

[44] Liu H, Zhang P, Zhang C, Chen J, Jiang J-H. Self-assembly of a dual-targeting and self-calibrating ratiometric polymer nanoprobe for accurate hypochlorous acid imaging. ACS Appl Mater Interfaces 2020;2:45822–9.

[45] Malkondu S, Erdemir S, Karakurt S. Red and blue emitting fluorescent probe for cyanide and hypochlorite ions: biological sensing and environmental analysis. Dyes Pigments 2020;174. 108019.

[46] Chen X, Gao H, Deng Y, Jin Q, Ji J, Ding D. Supramolecular aggregation-induced emission nanodots with programmed tumor microenvironment responsiveness for image-guided orthotopic pancreatic cancer therapy. ACS Nano 2020;14:5121–34.

[47] Zhang Z, Zhao Z, Wu L, Lu S, Ling S, Li G, Xu L, Ma L, Hou Y, Wang X, Li X, He G, Wang K, Zou B, Zhang M. Emissive platinum(II) cages with reverse fluorescence resonance energy transfer for multiple sensing. J Am Chem Soc 2020;142:2592–600.

[48] Sun J, Hua B, Li Q, Zhou J, Yang J. Acid/base-controllable FRET and self-assembling systems fabricated by rhodamine B functionalized pillar[5]arene-based host-guest recognition motifs. Org Lett 2018;20:365–8.

[49] Sedgwick AC, Wu L, Han H-H, Bull SD, He X-P, James TD, Sessler JL, Tang BZ, Tian H, Yoon J. Excited-state intramolecular proton-transfer (ESIPT) based fluorescence sensors and imaging agents. Chem Soc Rev 2018;47:8842–80.

[50] Yuan X, Leng T-H, Guo Z-Q, Wang C-Y, Li J-Z, Yang W-W, Zhu W-H. A FRET-based dual-channel turn-on fluorescence probe for the detection of Hg^{2+} in living cells. Dyes Pigments 2019;161:403–10.

[51] Han T, Yuan Y, Kang H, Zhang Y, Dong L. Ultrafast, sensitive and visual sensing of copper ions by a dual-fluorescent film based on quantum dots. J Mater Chem C 2019;7:14904–12.

[52] Xu H, Zhu C, Chen Y, Bai Y, Han Z, Yao S, Jiao Y, Yuan H, He W, Guo Z. A FRET-based fluorescent Zn^{2+} sensor: 3D ratiometric imaging, flow cytometric tracking and cisplatin-induced Zn^{2+} fluctuation monitoring. Chem Sci 2020;11:11037–104.

[53] Wu L, Huang C, Emery BP, Sedgwick AC, Bull SD, He XP, Tian H, Yoon J, Sessler JL, James TD. Förster resonance energy transfer (FRET)-based small-molecule sensors and imaging agents. Chem Soc Rev 2020;49:5110–39.

[54] Kan A, Liu X, Xu X, Zhang N, Jiang W. A bimolecular i-motif mediated FRE strategy for imaging protein homodimerization on a living tumor cell surface. Chem Commun 2020;56:13405–8.
[55] Wang Z, He X, Yong T, Miao Y, Zhang C, Tang BZ. Multicolor tunable polymeric nanoparticle from the tetraphenylethylene cage for temperature sensing in living cells. J Am Chem Soc 2020;142:512–9.
[56] Wang W, Li N, Liu J-T, Miao J-Y, Zhao B-X, Lin Z-M. A new FRET-based ratiometric fluorescent probe for the detection of SO_2 derivatives in mitochondria of living cells. Dyes Pigments 2020;181. 108639.
[57] Wang L, Cao H-X, He Y-S, Pan C-G, Sun T-K, Zhang X-Y, Wang CY, Liang G-X. Facile preparation of amino-carbon dots/gold nanoclusters FRET ratiometric fluorescent probe for sensing of Pb^{2+}/Cu^{2+}. Sensor Actuator B Chem 2019;282:78–84.